Research Square

Preprints are preliminary reports that have not undergone peer review.
They should not be considered conclusive, used to inform clinical practice,
or referenced by the media as validated information.

Influence of annealing temperature on the structural, morphological and optical properties of sol–gel spin-coated NiO thin films on Si and SiO_2 substrates

Javohir Sh Khudoykulov
xjavokhir1799@gmail.com

National University of Uzbekistan
Shavkat U Yuldashev
National University of Uzbekistan
Azamat O Arslanov
National University of Uzbekistan
Jamoliddin X Murodov
Center for Nanotechnologies Development, National University of Uzbekistan
Noiba U Botirova
Center for Nanotechnologies Development, National University of Uzbekistan
Ilyos Kh Khudaykulov
Institute of Ion Plasma Laser Technologies
Marguba Sh Azimova
National University of Uzbekistan

Research Article

Keywords: NiO thin films, sol–gel spin coating, annealing temperature, X-ray diffraction, optical band gap, Urbach energy

Posted Date: September 16th, 2026

DOI: https://doi.org/10.21203/rs.3.rs-10346476/v1

License: This work is licensed under a Creative Commons Attribution 4.0 International License.
Read Full License

Additional Declarations: No competing interests reported.

Version of Record: A version of this preprint was published at Journal of Materials Science: Materials in Electronics on October 26th, 2026. See the published version at https://doi.org/10.1007/s10854-026-18739-y.

Abstract

Nanocrystalline nickel oxide (NiO) thin films were deposited on Si and thermally oxidized SiO_2 substrates by sol–gel spin coating and subsequently annealed in air at 400, 500 and 600°C for 1 h. The influence of the post-deposition annealing temperature on the structural, morphological and optical properties of the films was investigated by X-ray diffraction (XRD), scanning electron microscopy (SEM) and ultraviolet–visible (UV–Vis) spectroscopy. All annealed films crystallize in the cubic rock-salt NiO phase (JCPDS 00-047-1049) with (111) and (200) reflections and no secondary phases. Increasing the annealing temperature from 400 to 600°C sharpens both reflections: the Scherrer crystallite size increases from ≈ 4–6 nm to ≈ 10–11 nm, while the microstrain and dislocation density decrease by a factor of about three, and the lattice parameter relaxes towards the bulk NiO value (a ≈ 4.18 Å). Cross-sectional SEM gives film thicknesses of 166 nm (Si) and 187 nm (SiO_2), and the 600°C films exhibit dense, crack-free, fine-grained surfaces. The direct optical band gap increases from 3.42 to 3.55 eV on Si and remains at 3.63–3.66 eV on SiO_2, while the Urbach energy decreases from 108 to 82 meV (Si) and from 155 to 67 meV (SiO_2), correlating with the improved crystallinity. The results identify 600°C as the optimum annealing temperature for producing well-crystallized NiO films with low structural disorder.

1. Introduction

Nickel oxide (NiO) is one of the few binary oxide semiconductors that exhibits intrinsic p-type conductivity, which it combines with a wide direct band gap (3.4–4.0 eV), high chemical and thermal stability, and a large exciton binding energy [1–3]. Owing to this rare combination of properties, NiO thin films have been employed as hole-transport and electron-blocking layers in perovskite and organic solar cells, as electrochromic and smart-window electrodes, and in resistive switching memories, gas sensors and UV photodetectors [1, 4–6]. The p-type character of NiO originates predominantly from nickel vacancies and the associated Ni^{3+} states, so that the electrical and optical response of a given film is extremely sensitive to its defect chemistry and microstructure [7, 8].

Among the numerous deposition routes reported for NiO — sputtering, pulsed laser deposition, chemical bath deposition, spray pyrolysis and sol–gel processing — the sol–gel spin-coating technique is particularly attractive because it is vacuum-free, inexpensive, easily scalable, and provides straightforward control over the precursor chemistry and film thickness [3, 5, 11]. In sol–gel derived films, however, the final film properties are established during the post-deposition heat treatment, when the residual organics decompose, the amorphous gel network converts to the oxide, and crystallite growth, densification and defect annihilation take place. The annealing temperature is therefore the single most influential processing parameter [12]. It has been shown to govern the crystallite size, texture, surface morphology, stoichiometry, band gap and conductivity of NiO films prepared by sol–gel and related chemical methods [1, 2, 5, 9].

Several groups have examined the effect of annealing temperature on sol–gel NiO films deposited on glass, quartz or transparent conducting substrates [1, 2, 5, 6]. Considerably less attention has been paid

to films grown directly on crystalline Si and on thermally oxidized SiO_2/Si — the two technologically most relevant platforms for the monolithic integration of NiO-based photodetectors, memristive devices and heterojunction diodes [4]. Because the substrate controls the nucleation density, the film–substrate thermal-expansion mismatch and the interfacial chemistry, the evolution of the film microstructure with annealing temperature cannot be assumed to be substrate-independent. A direct, side-by-side comparison of the annealing behaviour of identically prepared NiO films on Si and SiO_2 is still scarce in the literature.

In the present work, NiO thin films were deposited simultaneously on Si and SiO_2 substrates by sol–gel spin coating and annealed at 400, 500 and 600°C in a muffle furnace in ambient air. The structural evolution (phase, crystallite size, microstrain, dislocation density, lattice parameter and texture), the surface and cross-sectional morphology, and the optical characteristics (absorption edge, direct band gap and Urbach energy) were studied systematically as functions of the annealing temperature for both substrates, and the correlations between the structural and optical parameters are discussed. The combined data set allows the optimum annealing window for device-quality NiO films on silicon-based substrates to be identified.

2. Experimental details

2.1. Film preparation

NiO thin films were fabricated on Si and thermally oxidized SiO_2/Si substrates by the sol–gel spin-coating technique. Nickel acetate tetrahydrate ($Ni(CH_3COO)_2 \cdot 4H_2O$) was used as the nickel precursor and 2-methoxyethanol as the solvent. A 0.5 M precursor solution was prepared, and ethanolamine (EA) was added as a stabilizing agent in an equimolar (1:1) ratio with respect to the nickel precursor. The solution was magnetically stirred at 60°C for 2 h to obtain a clear, homogeneous sol, which was subsequently aged for 48 h at room temperature to promote complete gel formation and to improve its stability prior to deposition.

Before deposition, the Si and SiO_2 substrates were thoroughly cleaned following a conventional cleaning procedure. The aged sol was spin-coated onto the substrates at 3000 rpm for 30 s. To reach the desired film thickness the coating cycle was repeated ten times, and after each cycle the deposited layer was pre-annealed at 250°C for 15 min to evaporate residual solvents, remove organic components and densify the oxide network. Finally, the films were annealed in ambient air at 400, 500 and 600°C for 1 h using a heating rate of 10°C min^{-1}. A schematic diagram of the deposition sequence is shown in Fig. 1.

2.2. Characterization

The crystalline structure of the films was analysed by Smartlab Se X-ray diffractometer (XRD) equipped with Cu Kα radiation (λ = 1.5406 Å); the patterns were recorded over the 2θ range 10–60° with a step of 0.02°. Diffraction patterns of the bare Si and SiO_2 substrates were collected under identical conditions

and used as background references. The surface morphology and the film cross-sections were examined by scanning electron microscopy (SEM) at an accelerating voltage of 20 kV using secondary-electron (ETD) and concentric backscattered (CBS) detectors at magnifications of 120,000–250,000×. Optical absorbance spectra were recorded in the 200–600 nm wavelength range. Yoke M601S-X model used for optical measurments.

2.3. Data analysis

The NiO (111) and (200) reflections were fitted with Gaussian profiles on a constant background. In the 42–45.6° window a two-component fit was used in order to separate the broad NiO (200) reflection from a narrow substrate-related feature at 2θ ≈ 44.3° that is also present in the patterns of the bare substrates. The average crystallite size D was evaluated from the full width at half maximum (FWHM, β) of the reflections using the Scherrer equation:

$D = K\lambda / (\beta \cos\theta)$ (1)

with the shape factor K = 0.9. The microstrain was estimated as:

$\varepsilon = \beta / (4 \tan\theta)$ (2)

and the dislocation density as:

$\delta = 1 / D^2$ (3)

The texture coefficient was calculated as:

$TC(hkl) = [I(hkl)/I_0(hkl)] / [N^{-1}\Sigma\, I(hkl)/I_0(hkl)]$ (4)

where I and I_0 are the measured and JCPDS 00-047-1049 reference intensities and N = 2 is the number of analysed reflections. No correction for instrumental broadening was applied, so the quoted crystallite sizes represent lower-bound estimates; a Williamson–Hall analysis was not attempted because only two NiO reflections are available within the measured angular range.

The absorption coefficient was obtained from the measured absorbance A and the SEM-determined film thickness t as:

$\alpha = 2.303A / t$ (5)

The direct optical band gap was determined from Tauc plots, $(\alpha h\nu)^2$ versus hν, by extrapolating the linear portion of the absorption edge to $(\alpha h\nu)^2 = 0$, as appropriate for a direct allowed transition in NiO [10, 11]. The Urbach energy E_U was extracted from the slope of ln(α) versus hν in the exponential sub-gap region, following:

$\alpha = \alpha_0 \exp(h\nu / E_U)$ [12] (6)

3. Results and discussion

3.1. Structural properties (XRD)

Figure 2 shows the XRD patterns of the NiO films annealed at 400, 500 and 600°C on SiO_2 (Fig. 2a) and Si (Fig. 2b), together with the patterns of the corresponding bare substrates. All annealed films exhibit reflections at 2θ ≈ 37.1° and ≈ 43.2°, which are indexed as the (111) and (200) planes of cubic rock-salt NiO (space group Fm-3m, JCPDS 00-047-1049) [14]. Reflections attributable to $Ni(OH)_2$, Ni_2O_3 or metallic Ni are not detected, confirming that a single-phase NiO film is obtained at all annealing temperatures. The sharp features at 2θ ≈ 32.9°, 44.3° and 56.2° are also present in the bare-substrate patterns and are therefore substrate-related artefacts; the narrow 44.3° peak was explicitly deconvoluted from the neighbouring NiO (200) reflection in the quantitative analysis (Section 2.3).

The evolution of the line profiles with annealing temperature reveals a clear crystallization sequence. After annealing at 400°C the NiO reflections are extremely broad and weak — the (111) line cannot be resolved reliably above the noise level — indicating an essentially X-ray-amorphous to nanocrystalline film at the onset of crystallization. At 500°C both reflections become distinct, and at 600°C they are well developed and considerably narrowed on both substrates. The quantitative results of the profile analysis are collected in Table 1.

The Scherrer crystallite size obtained from the (200) reflection increases from 3.6 nm (400°C) to 8.8 nm (500°C) and 10.5 nm (600°C) for the films on Si, and from 6.3 nm (400°C) to 10.4 nm (600°C) for the films on SiO_2, with consistent values (10.3–11.0 nm) obtained from the (111) reflection at 600°C. The growth of the crystallites is accompanied by a systematic decrease of the microstrain from ≈(15–26)×10^{-3} at 400°C to ≈(9–10)×10^{-3} at 600°C and by an almost order-of-magnitude reduction of the dislocation density (Table 1). This behaviour reflects the thermally activated coalescence of neighbouring crystallites and the annihilation of grain-boundary defects, in agreement with previous reports on sol–gel NiO films annealed in a comparable temperature window [1, 2, 5]. It should be noted that the film on SiO_2 annealed at 500°C shows an anomalously weak and broad (200) reflection, so the corresponding parameters carry a large uncertainty; the (111)-based values (D ≈ 7.6 nm) are considered more representative for this sample. This retarded intermediate-stage crystallization on the amorphous oxide may reflect the lower nucleation density on SiO_2 compared with crystalline Si, although a sample-to-sample variation cannot be excluded on the basis of a single specimen.

The lattice parameter calculated from the (200) spacing increases on Si (4.163 → 4.181 Å) and relaxes slightly on SiO_2 (4.184 → 4.182 Å) as the annealing temperature is raised, in both cases approaching the bulk NiO value of 4.177 Å [14]. The deviation of the lattice parameter from the bulk value at low annealing temperature, together with the high microstrain, indicates a defective, strained lattice — commonly associated in NiO with excess oxygen/nickel-vacancy disorder and residual stress — which is progressively relieved during high-temperature annealing [1, 7]. The texture coefficients at 500–600°C show a mild preferential (200) orientation, TC(200) ≈ 1.15–1.21, which strengthens with annealing

temperature on both substrates. A preferred (200) orientation is frequently observed in annealed rock-salt oxide films because {100} facets have the lowest surface energy in the NaCl-type structure, so grains bounded by {100} planes grow at the expense of other orientations during coarsening [2, 5]. With only two reflections available, however, these TC values should be regarded as indicative.

Table 1
Structural parameters of the NiO films obtained from the Gaussian profile analysis of the (111) and (200) reflections: peak position 2θ, FWHM, interplanar spacing d, lattice parameter a, Scherrer crystallite size D, microstrain ε, dislocation density δ and texture coefficient TC. Numbers in parentheses are the fit standard errors in the last digit(s); "n.r." — not resolved.

Sample	(hkl)	2θ (°)	FWHM (°)	d (Å)	a (Å)	D (nm)	ε (10^{-3})	δ (10^{-3} nm^{-2})	TC(hkl)
SiO_2 / 400°C	(111)	n.r.	n.r.	–	–	–	–	–	–
	(200)	43.21(3)	1.35(9)	2.0919	4.184	6.3	14.9	25.0	–
SiO_2 / 500°C	(111)	36.88(5)	1.10(14)	2.4355	4.218	7.6	14.4	17.3	1.15
	(200)	43.04(12)	2.16(56)	2.0998	4.200	3.9	23.9	63.8	0.85
SiO_2 / 600°C	(111)	37.14(3)	0.76(7)	2.4190	4.190	11.0	9.9	8.2	0.82
	(200)	43.23(1)	0.82(4)	2.0911	4.182	10.4	9.1	9.3	1.18
Si / 400°C	(111)	n.r.	n.r.	–	–	–	–	–	–
	(200)	43.44(5)	2.37(31)	2.0817	4.163	3.6	25.9	76.5	–
Si / 500°C	(111)	37.13(2)	0.81(6)	2.4196	4.191	10.4	10.5	9.3	0.85
	(200)	43.27(2)	0.97(5)	2.0892	4.179	8.8	10.7	13.0	1.15
Si / 600°C	(111)	37.17(3)	0.81(7)	2.4167	4.186	10.3	10.5	9.4	0.79
	(200)	43.24(1)	0.82(3)	2.0906	4.181	10.5	9.0	9.1	1.21

3.2. Surface morphology and cross-section (SEM)

Figure 3 presents the plan-view SEM micrographs of the films annealed at 600°C, which are shown as representative of the film morphology; SEM imaging was performed for the 600°C samples only. Both films display a continuous, dense and crack-free surface built of fine, roundish grains and grain agglomerates with apparent lateral sizes of roughly 10–25 nm. This scale is consistent with the XRD crystallite size of ≈ 10–11 nm at 600°C, suggesting that the visible surface features correspond to individual crystallites or small agglomerates of two to three crystallites. No pinholes, droplets or cracks

are observed at magnifications up to 250,000×, confirming that the repeated coating/pre-annealing protocol yields homogeneous coverage on both substrates.

The cross-sectional micrographs are shown in Fig. 4. On SiO_2 (Fig. 4a), the backscattered-electron (CBS) image provides strong compositional contrast: the NiO layer appears as a bright, uniform band of 186.6 nm thickness on top of the darker 134.9 nm thermally grown SiO_2 layer, with sharp, well-defined interfaces and no visible interfacial voids or delamination. On Si (Fig. 4b), the film thickness measured from the secondary-electron image is 166.4 nm, and the layer is compact and featureless across the imaged region, without columnar voids or layering artefacts from the multi-step deposition. The average thickness increment per coating cycle is therefore ≈ 17–19 nm, demonstrating good run-to-run reproducibility of the spin-coating/pre-annealing sequence. The measured thicknesses were used for the calculation of the absorption coefficient in Section 3.3.

3.3. Optical properties (UV–Vis, Tauc and Urbach analysis)

The direct band gap was evaluated from the Tauc plots shown in Fig. 5, and the Urbach energies from the semilogarithmic plots in Fig. 6; the resulting parameters are summarized in Table 2. For the films on Si, E increases monotonically from 3.42 eV (400°C) to 3.48 eV (500°C) and 3.55 eV (600°C). For the films on SiO_2 the gap stays within a narrow window of 3.63–3.66 eV, with no monotonic trend. All values fall inside the 3.4–3.9 eV range commonly reported for nanocrystalline NiO films [1, 3, 5, 9].

Two observations deserve comment. First, the band-gap widening on Si with increasing annealing temperature occurs while the crystallite size increases, which rules out quantum confinement as its origin (confinement would produce the opposite trend). A more plausible explanation is the progressive narrowing of the band-tail and defect-state distribution near the band edges: as the Ni^{3+}/vacancy-related disorder is annealed out, the effective absorption onset moves towards the intrinsic gap [1, 7]. This interpretation is directly supported by the simultaneous decrease of the Urbach energy from 108 to 82 meV on Si. We emphasize, however, that the E–D correlation established here does not by itself prove causality, and complementary compositional probes (e.g. XPS of the Ni^{3+}/Ni^{2+} ratio) would be required for a definitive assignment. Second, the films on SiO_2 exhibit systematically larger E (by 0.1–0.2 eV) and, at 400–500°C, larger E than the films on Si. A contribution of substrate-dependent measurement conditions and interference effects to this offset cannot be excluded, since the absorbance of films on the two different stacks is not strictly comparable; the substrate-dependent microstructure evidenced by XRD (Section 3.1) is expected to contribute as well.

The Urbach energy decreases with annealing temperature on both substrates — from 108 to 82 meV on Si and from 155 to 67 meV on SiO_2 — mirroring the decrease of the XRD microstrain and dislocation density (Table 1). Since $E_$ measures the exponential tailing of the density of states caused by structural disorder [13], its reduction confirms at the optical level the defect annihilation inferred from the diffraction data. The lowest disorder ($E_$ = 67–82 meV) is reached after annealing at 600°C, which, combined with the largest crystallite size, the near-bulk lattice parameter and the dense crack-free

morphology, identifies 600°C as the optimum annealing temperature within the studied window. It should be noted that the sub-gap absorption from which E□ is extracted may contain a residual contribution from interference fringes; the fitted ranges were therefore restricted to the steep edge region immediately below the gap, where the exponential behaviour is well obeyed ($R^2 \geq 0.96$, Table 2).

Table 2
Optical parameters of the NiO films: approximate absorption-edge wavelength, direct band gap E□ from the Tauc analysis, Urbach energy E□, and the coefficients of determination of the corresponding linear fits.

Sample	Absorption edge (nm)	E□ (eV)	R^2 (Tauc fit)	E□ (meV)	R^2 (Urbach fit)
Si / 400°C	≈ 363	3.42	0.993	108	1.000
Si / 500°C	≈ 357	3.48	0.990	81	0.999
Si / 600°C	≈ 350	3.55	0.991	82	0.999
SiO_2 / 400°C	≈ 342	3.63	0.998	155	0.963
SiO_2 / 500°C	≈ 339	3.66	0.996	128	0.971
SiO_2 / 600°C	≈ 341	3.64	0.999	67	0.996

4. Conclusions

NiO thin films were grown on Si and SiO_2 substrates by sol–gel spin coating (ten coating cycles, 0.5 M nickel acetate sol) and annealed in air at 400–600°C for 1 h. XRD shows that all films crystallize in the single-phase cubic rock-salt structure of NiO with (111) and (200) reflections. Raising the annealing temperature from 400 to 600°C increases the Scherrer crystallite size from ≈ 4–6 nm to 10.3–11.0 nm, reduces the microstrain from $\approx(15–26)\times10^{-3}$ to $\approx(9–10)\times10^{-3}$ and the dislocation density from $\approx(25–77)\times10^{-3}$ nm^{-2} to $\approx 9\times10^{-3}$ nm^{-2}, and drives the lattice parameter towards the bulk value (≈ 4.18 Å), with a mild (200) texture developing at 600°C. SEM of the 600°C films reveals dense, crack-free surfaces with ≈ 10–25 nm features and sharp film/substrate interfaces, with thicknesses of 166.4 nm on Si and 186.6 nm on SiO_2. The direct band gap increases from 3.42 to 3.55 eV on Si and remains at 3.63–3.66 eV on SiO_2, while the Urbach energy decreases to 67–82 meV at 600°C on both substrates, in quantitative agreement with the structural ordering. Annealing at 600°C thus yields the best-crystallized, least-disordered NiO films in the investigated range and is recommended for silicon-integrated NiO device layers.

Declarations

Competing interests

The authors declare that they have no known competing financial interests or personal relationships that could have appeared to influence the work reported in this paper.

Funding

This research received no external funding.

Author Contribution

Author ContributionsShavkat U. Yuldashev: Supervision.Azamat O. Arslanov: Formal analysis; (Fig. 5, Tauc plot analysis).Jamoliddin X. Murodov: Formal analysis; Visualization (Fig. 2, XRD pattern analysis and plotting).Noiba U. Botirova: Formal analysis (structural and optical parameter calculations presented in Table 1 and Table 2).Ilyos Kh. Khudaykulov: Investigation (X-ray diffraction measurements).Marguba Sh. Azimova: Investigation; Resources (substrate preparation and thermal oxidation process).All authors have read and agreed to the published version of the manuscript.

Availability of data and materials

The datasets generated and analysed during the current study are available from the corresponding author on reasonable request.

References

1. N.R. Aswathy, J. Varghese, R. Vinodkumar, Effect of annealing temperature on the structural, optical, magnetic and electrochemical properties of NiO thin films prepared by sol–gel spin coating. J. Mater. Sci. : Mater. Electron. **31**, 16634–16648 (2020). https://doi.org/10.1007/s10854-020-04218-5
2. T. Ivanova, A. Harizanova, M. Shipochka, P. Vitanov, Nickel oxide films deposited by sol-gel method: effect of annealing temperature on structural, optical, and electrical properties. Materials. **15**, 1742 (2022). https://doi.org/10.3390/ma15051742
3. A.A. Al-Ghamdi, W.E. Mahmoud, S.J. Yaghmour, F.M. Al-Marzouki, Structure and optical properties of nanocrystalline NiO thin film synthesized by sol–gel spin-coating method. J. Alloys Compd. **486**, 9–13 (2009). https://doi.org/10.1016/j.jallcom.2009.06.139
4. M.H. Mohsin, M.J. Haider, Z.Y.A. Al-Shibaany, A.J. Haider, R.O. Mehadi, Synthesis of NiO/Si using sol-gel as a photosensor. Silicon. **14**, 1349–1355 (2022). https://doi.org/10.1007/s12633-020-00872-w
5. M. Martínez-Gil, M.I. Pintor-Monroy, M. Cota-Leal, D. Cabrera-German, A. Garzon-Fontecha, M.A. Quevedo-López, M. Sotelo-Lerma, Influence of annealing temperature on nickel oxide thin films grown by chemical bath deposition. Mater. Sci. Semicond. Process. **72**, 37–45 (2017). https://doi.org/10.1016/j.mssp.2017.09.021
6. T. Ivanova, A. Harizanova, N. Petkov, Optical, electrical, and structural properties of NiO thin films, derived by sol–gel method. Gels. **11**, 944 (2025). https://doi.org/10.3390/gels11120944
7. R. Karsthof, Y.K. Frodason, A. Galeckas, P.M. Weiser, V. Zviagin, M. Grundmann, Light absorption and emission by defects in doped nickel oxide. Adv. Photonics Res. **3**, 2200138 (2022).

https://doi.org/10.1002/adpr.202200138

8. A.C. Gandhi, S.Y. Wu, Strong deep-level-emission photoluminescence in NiO nanoparticles. Nanomaterials. **7**, 231 (2017). https://doi.org/10.3390/nano7080231
9. S. Roguai, Tunable structural, optical, and photocatalytic properties of sulfur-doped NiO thin films: influence of doping concentration and scavenger-assisted mechanism analysis. J. Sol-Gel Sci. Technol. **117**, 46 (2026). https://doi.org/10.1007/s10971-025-07052-5
10. J. Tauc, R. Grigorovici, A. Vancu, Optical properties and electronic structure of amorphous germanium. Phys. Status Solidi B **15**, 627–637 (1966). https://doi.org/10.1002/pssb.19660150224
11. N.V. Srinivasa, K. Haunsbhavi, N. Srinatha, H.M. Mahesh, B. Angadi, Preparation and characterization of Sn doped NiO thin films by sol–gel spin coating technique, Mater. Today Proc. (2023). https://doi.org/10.1016/j.matpr.2023.05.597
12. U. Noiba, A.O. Botirova, G.B. Arslanov, X. Eshonkulov, Jamoliddin, Murodov, Ra'no Sh. Sharipova, Javohir Sh. Khudoykulov, and Shavkat U. Yuldashev. EffectofSiO2 andPost-AnnealedGa2O3 BufferLayersonGa2O3 Thin Film Growth and Properties // Crystal Growth & Design. https://doi.org/10.1021/acs.cgd.5c01075
13. F. Urbach, The long-wavelength edge of photographic sensitivity and of the electronic absorption of solids. Phys. Rev. **92**, 1324–1330 (1953). https://doi.org/10.1103/PhysRev.92.1324
14. Joint Committee on Powder Diffraction Standards (JCPDS), Card No. 00-047-1049 (NiO, bunsenite), International Centre for Diffraction Data (ICDD), Newtown Square, PA

Figures

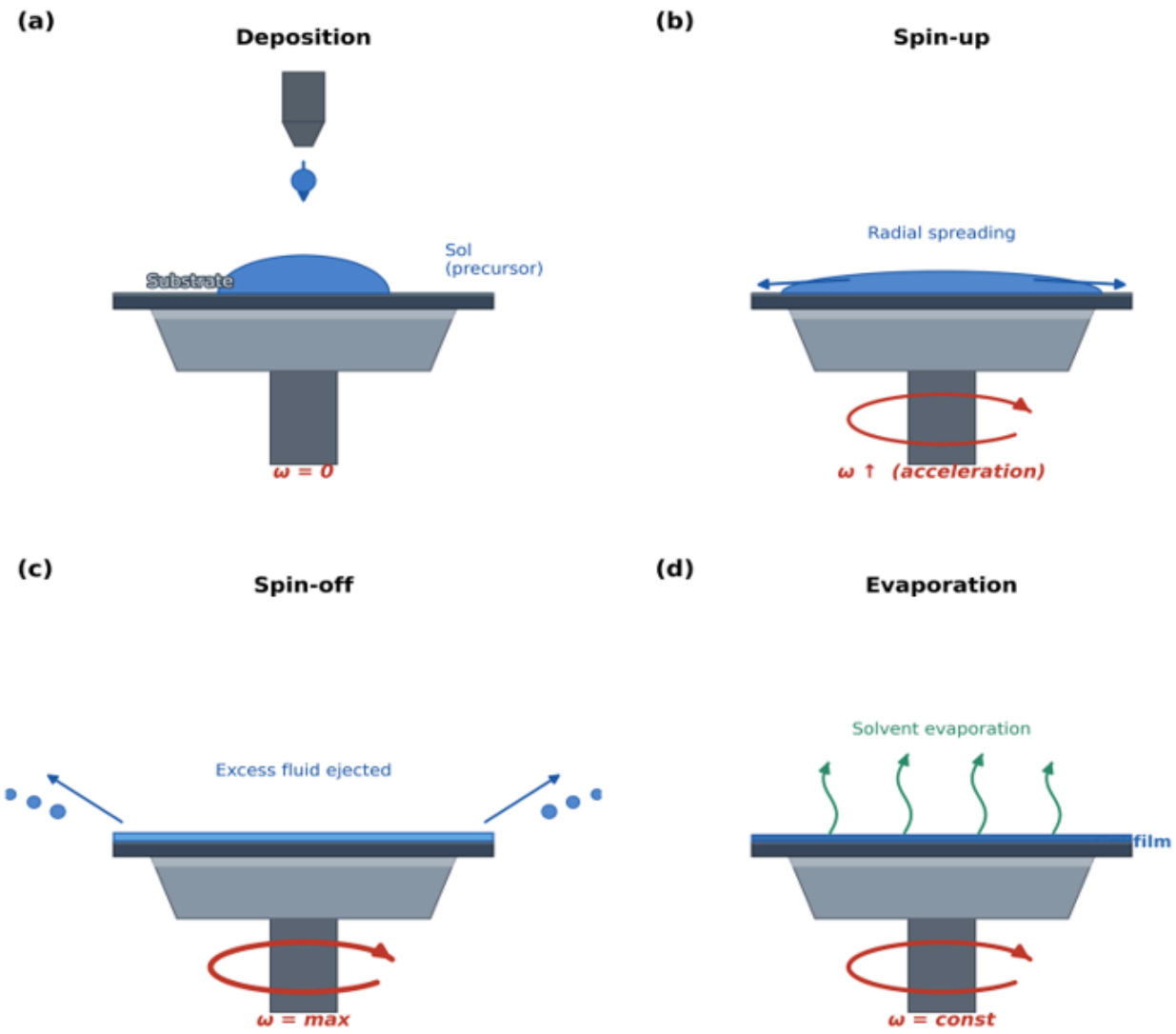


Figure 1

Schematic illustration of the sol–gel spin-coating procedure used for the deposition of the NiO thin films:

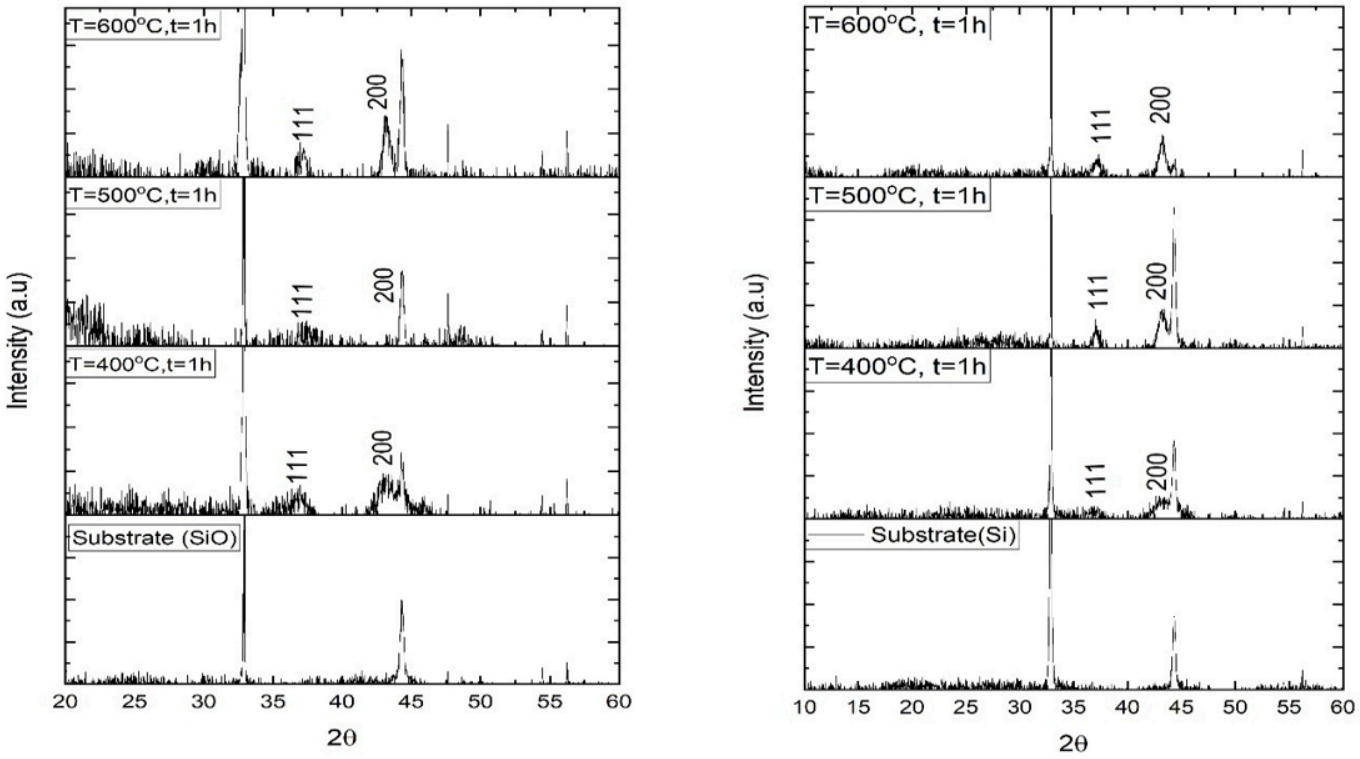


Figure 2

XRD patterns (Cu Kα) of the NiO thin films annealed at 400, 500 and 600 °C for 1 h on (a) SiO_2 and (b) Si substrates; the bottom curves show the corresponding bare-substrate patterns. The NiO (111) and (200) reflections of the cubic rock-salt phase (JCPDS 00-047-1049) are indexed; the unlabelled sharp features (≈32.9°, 44.3°, 56.2°) originate from the substrates.

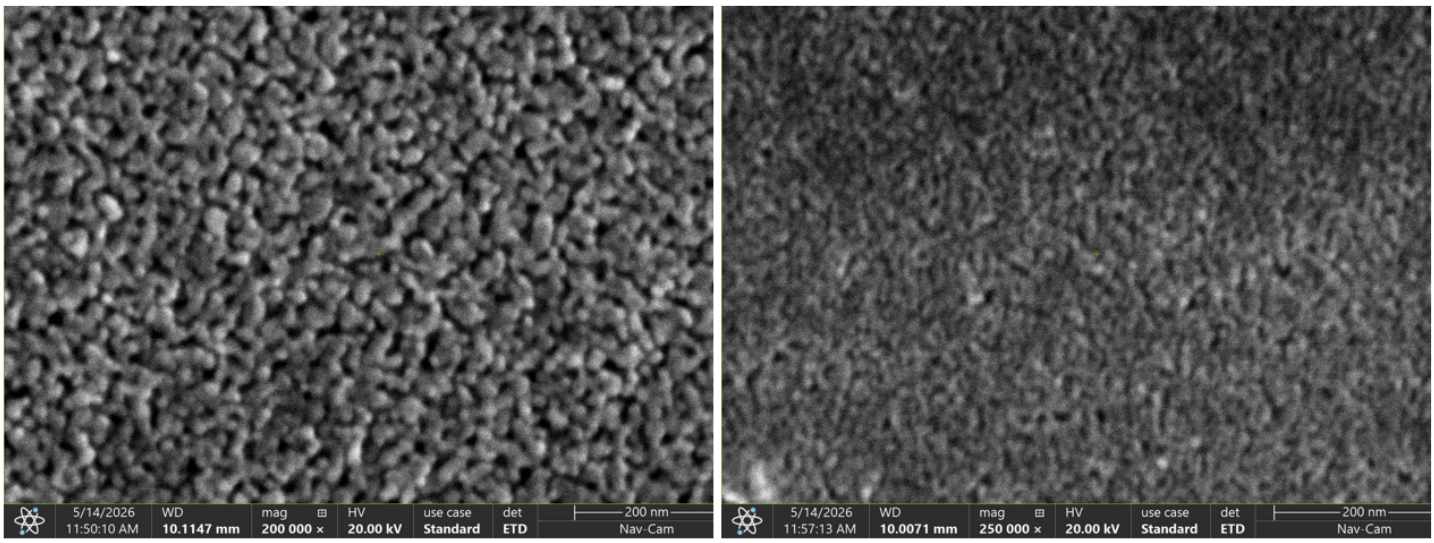


Figure 3

Representative plan-view SEM micrographs of the NiO films annealed at 600 °C on (a) SiO_2 (200,000×) and (b) Si (250,000×), recorded at 20 kV with the ETD detector. Both films show a dense, crack-free, fine-grained morphology with apparent feature sizes of ≈10–25 nm.

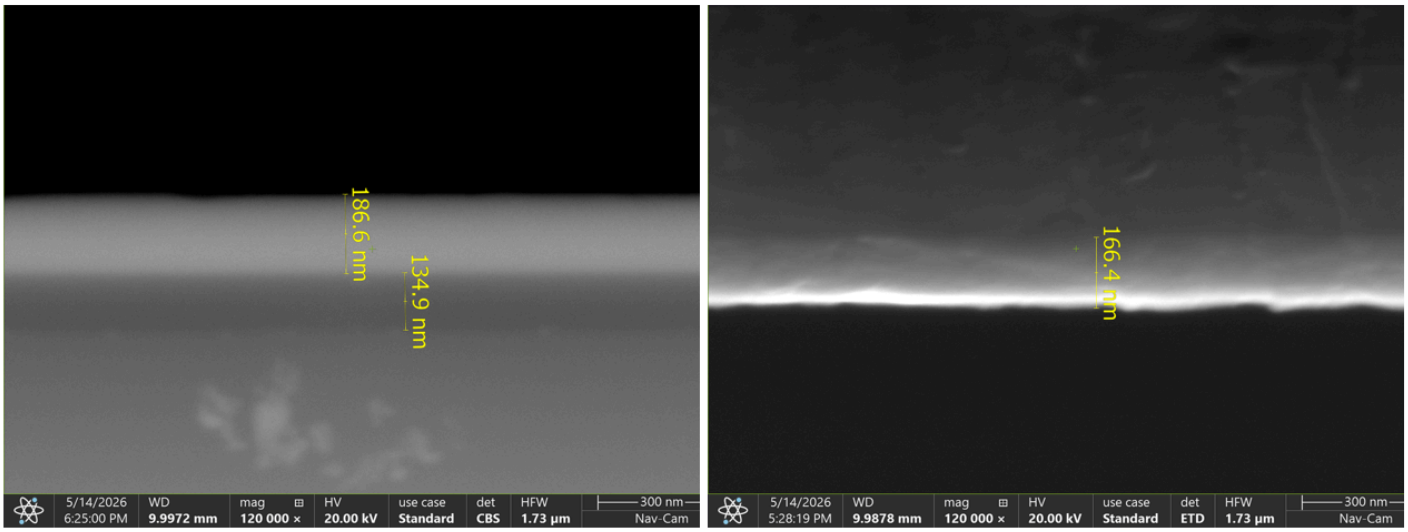


Figure 4

Cross-sectional SEM micrographs of the 600 °C-annealed films: (a) $NiO/SiO_2/Si$ stack imaged with the backscattered-electron (CBS) detector — the bright NiO layer (186.6 nm) is clearly distinguished from the 134.9 nm thermally grown SiO_2 layer; (b) NiO film on Si imaged with the ETD detector, giving a film thickness of 166.4 nm.

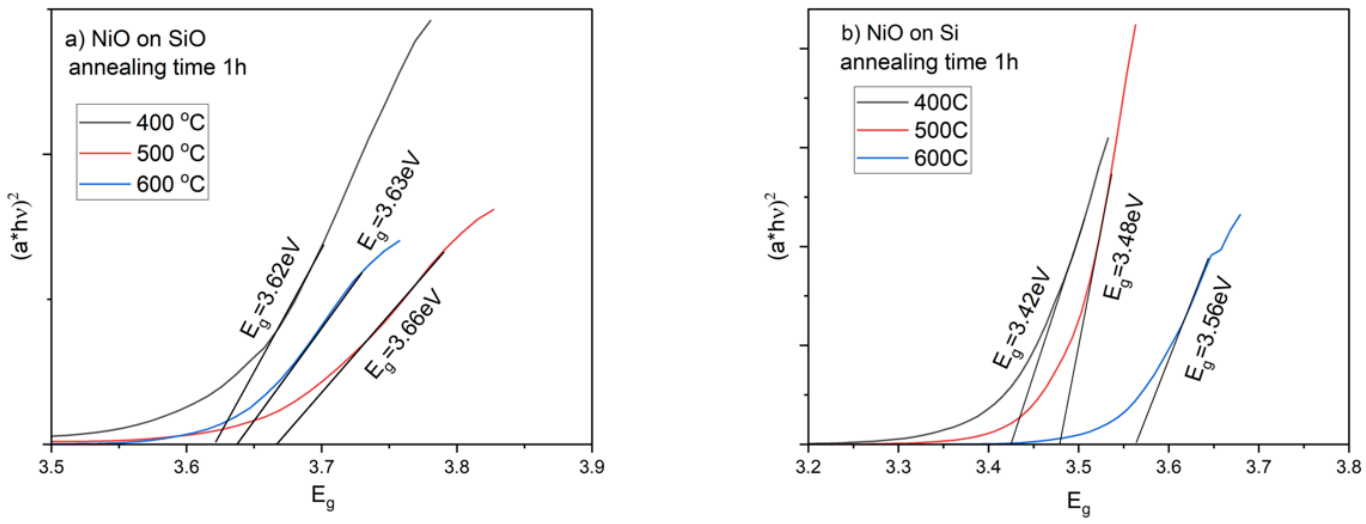


Figure 5

Tauc plots, $(\alpha h\nu)^2$ versus photon energy, for the direct allowed transition of the NiO films on (a) SiO_2 and (b) Si. Extrapolation of the linear edge regions (solid lines) yields the band gaps listed in Table 2.

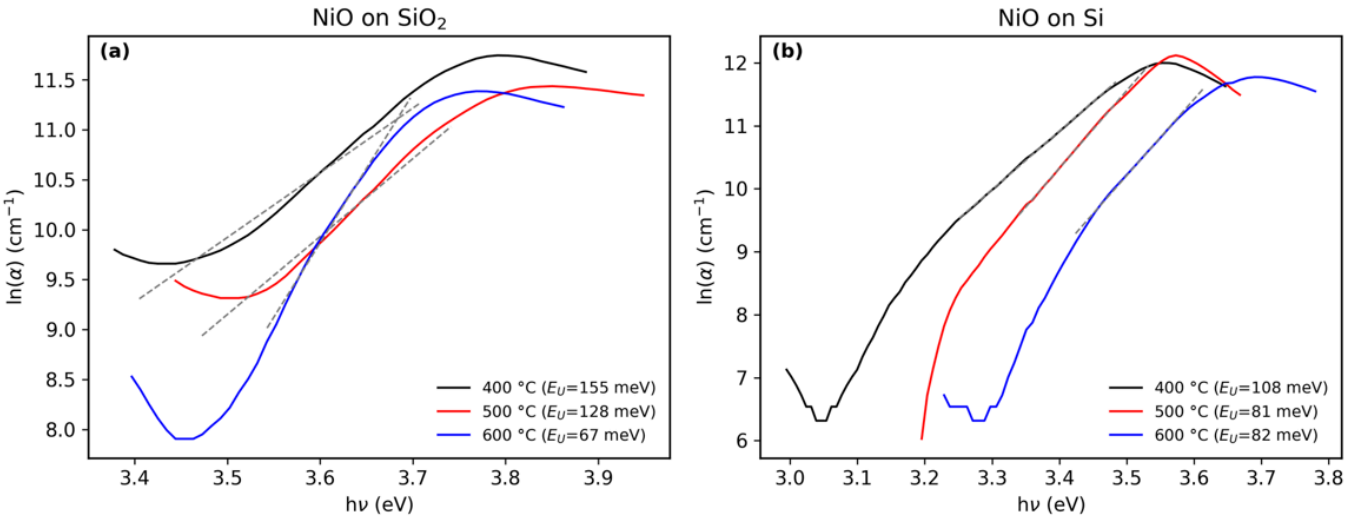


Figure 6

Urbach plots, ln(α) versus photon energy, for the NiO films on (a) SiO_2 and (b) Si; dashed lines show the linear fits in the exponential sub-gap region used to extract the Urbach energies E given in Table 2.